Current Biology 16, 1685–1693, September 5, 2006 ©2006 Elsevier Ltd All rights reserved DOI 10.1016/j.cub.2006.07.056

Article

Potential for Control of Signaling Pathways via Cell Size and Shape

Jason Meyers,[1,2] Jennifer Craig,[1,2] and David J. Odde[1,*]

[1] Department of Biomedical Engineering
University of Minnesota
Minneapolis, Minnesota 55455

Summary

Background: In order for signals generated at the plasma membrane to reach intracellular targets, activated messengers, such as G proteins and phosphoproteins, must diffuse through the cytoplasm. If the deactivators of these messengers, GTPase activating proteins (GAPs) and phosphatases, respectively, are sufficiently active in the cytoplasm, then the signal could in principle decay before reaching the target and a stable spatial gradient in phosphostate would be generated. Recent experiments document the existence of such gradients in living cells and suggest a role for them in mitotic spindle morphogenesis and cell migration. However, how such systems behave theoretically when embedded in a cell of varying size or shape has not been considered.

Results: Here we use a simple mathematical model to explore the theoretical consequences of a plasma membrane bound activator (i.e., guanine nucleotide exchange factor, GEF, or kinase) and a cytoplasmic deactivator (i.e., GAP or phosphatase), and we find that as a model cell grows, the substrate becomes progressively dephosphorylated as a result of decreased proximity to the activator. Conversely, as a cell spreads and flattens, the substrate becomes globally phosphorylated because of increased proximity of the substrate to the activator. Similarly, in the leading edge of polarized cells and in protrusions such as lamellipodia or filopodia, the substrate is highly phosphorylated. As a specific test of the model, we found that the experimentally observed preferential activation of the G protein Cdc42 in the periphery of fibroblasts that was recently reported is consistent with model predictions.

Conclusions: We conclude that cell-signaling pathways can theoretically be turned on and off, both locally and globally, in response to alterations in cell size and shape.

Introduction

It is now well accepted that extracellular morphogen gradients play a key role in embryonic tissue development [1, 2]. More recently it has been argued that intracellular morphogen gradients exist and that they play a key role in such processes as cell division and cell motility [3–11]. Spatial gradients in putative intracellular morphogens could be generated by spatially segregated, antagonistic reactions, such as the phosphorylation and dephosphorylation reactions mediated by kinases and phosphatases, respectively. Provided that the antagonistic kinase and the phosphatase are not colocalized, then there will exist a spatial gradient in the phosphostate of the substrate at steady state. Similarly, a spatially segregated guanine nucleotide exchange factor (GEF) and GTPase-activating protein (GAP) pair will establish a steady-state gradient in the GTP/GDP state of its monomeric G protein substrate. For simplicity, the present discussion will use the terminology of the kinase/phosphatase system but will be illustrated with the experimentally observed local and global activation of Cdc42, a G protein controlled by a GEF/GAP system, as recently reported by Nalbant et al. [12].

Once established, intracellular morphogen gradients could be used to define regions where specific enzymatic reactions may proceed, and other regions where they may not, as a function of their proximity to the kinase. For example, in the case of cell division, a recent study showed that dephosphorylated Op18/stathmin, which is known to promote microtubule disassembly, exists in mitotic cells at high concentration at the cell periphery and at low concentration in the vicinity of chromosomes [3]. The gradient in Op18/stathmin phosphorylation correlates well with the experimentally observed recruitment of microtubules to the mitotic spindle in the central region of the cell and is presumed to be mediated by a chromosome-associated kinase (e.g., Polo kinase) and cytoplasmic phosphatase (e.g., PP2A) [3]. In general, spatially segregated antagonistic reactions potentially enable the cell to spatially control enzymatic activities.

To be effective in establishing spatial control, gradients need to be exerted over subcellular dimensions. As shown theoretically by Brown and Kholodenko [11], the distance over which the spatial gradient in the concentration of the phosphorylated form of the substrate decays, $L_{gradient}$, is given by

$$L_{gradient} = \sqrt{\frac{D}{k_p}}, \quad (1)$$

where k_p is the first-order phosphatase reaction rate constant (typically 0.1–100 s^{-1} [11]), and D is the diffusion coefficient (typically 1–10 $\mu m^2/s$ for globular proteins [13, 14]). From these values, it is estimated that the decay length will vary from ~0.1 μm to 10 μm, sufficiently broad so as to potentially play a role in the behavior of a broad range of cell types, from bacteria to embryos. Recent experimental results confirm the existence of gradient decay lengths on the scale of ~1 μm in both *Xenopus* extracts and in living cells [3, 7]. More generally, the size of the gradient can be scaled by a distance characteristic of the cell size, R, to yield the Thiele modulus, Φ, given by

$$\Phi = \sqrt{\frac{k_p R^2}{D}} = \frac{R}{L_{gradient}}. \quad (2)$$

*Correspondence: oddex002@umn.edu
[2] These authors contributed equally to this work.

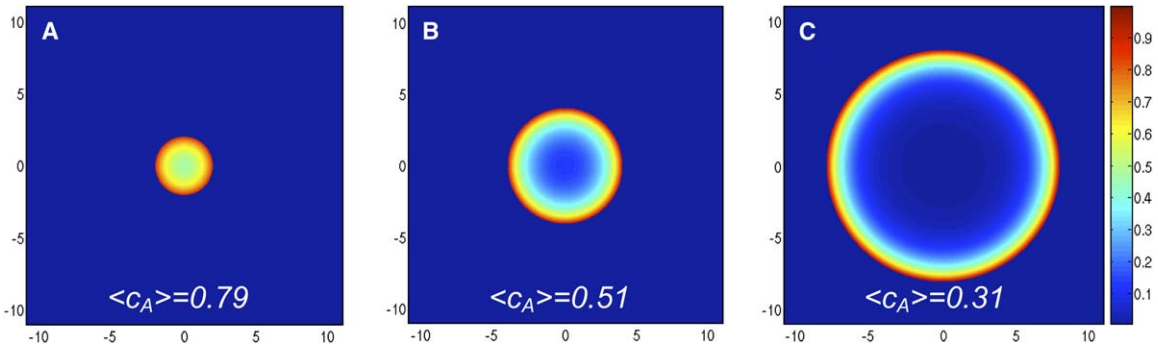

Figure 1. Increasing Cell Size Decreases Global Phosphorylation Levels

The concentration profile of the phosphorylated form of the substrate is shown for a planar slice through the center of a spherical cell. Parameters used: D = 10 $\mu m^2/s$, k_p = 10 s^{-1}, $L_{gradient}$ = 1 μm, k_{kin} = 50 s^{-1}, c_T = 1 μM.

(A) A small cell (radius = 2 μm) will be largely phosphorylated ($<c_A>$ = 0.79 μM) because the majority of the cytoplasm is within the gradient decay length ($L_{gradient}$) of the plasma membrane (Φ = 2).

(B) A slightly larger cell (radius = 4 μm) will be less phosphorylated ($<c_A>$ = 0.51 μM) because the cell size has increased while the gradient decay length has remained constant, so that a lesser fraction of the cytoplasm is within the gradient decay length of the plasma membrane (Φ = 4).

(C) A large cell (radius = 8 μm) will be mostly dephosphorylated ($<c_A>$ = 0.31 μM) because only a relatively small fraction of the cytoplasm is within the gradient decay length of the plasma membrane (Φ = 8). Thus, a 4-fold increase in cell radius results in 2.5-fold decrease in the average concentration of the phosphorylated form of the substrate, even as the activity levels of the kinase and phosphatase remain constant.

When $\Phi >> 1$, then the gradient decays very abruptly on the scale of the cell, and when $\Phi << 1$, then the gradient decays hardly at all on the scale of the cell. Thus, a third parameter that characterizes the diffusion-reaction system is size of the compartment in which the reactions occur. Although the theoretical possibility of intracellular phosphostate gradients has been appreciated [11], and two recent studies provide supporting experimental evidence [3, 7], the theoretical consequences of varying cell size and geometry have not been considered previously, even though cells come in a great variety shapes and sizes.

Here we analyze how phosphostate varies both globally and locally in response to changes in cell size and shape. From the analysis it becomes apparent that the physical size and shape of the cell are expected to be key influences that control whether a signaling cascade will be active, provided there is spatial segregation of the kinase and phosphatase. Specifically, in the case where the kinase is bound to the plasma membrane and the phosphatase is uniform in the cytoplasm, small and thin cells will be more phosphorylated than large and thick cells. The reason that large and thick cells fail to become activated is that there are large regions of the cytoplasm that are distant from the plasma membrane, thus making it very difficult for the phosphorylated form of the substrate to diffuse from the plasma membrane to distant regions without first being dephosphorylated by the phosphatase. The results may at least partially explain how cells are able to change their behavior as a function of cell shape [15, 16]. In general, the purpose of the analysis is not to explain how any particular signaling pathway operates, but rather to explore some of the generic responses of signaling systems that we might expect as they encounter normal changes in cell size and shape as mediated by the external mechanical environment and by the internal cytoskeleton as it generates forces to deform the cell. Nevertheless, we also specifically illustrate the behavior by comparison of model predictions of Cdc42 activation to recent experimental observations.

Results

To theoretically investigate the role of cell size and shape in controlling the phosphostate of the cell, we first considered the consequences of spherical cell size in the case where the kinase is attached to the plasma membrane and the phosphatase is located in the cytoplasm. As pointed out previously by Brown and Kholodenko [11], as the cell grows in size (i.e., as the radius R increases), the cell will experience a progressive decrease in the concentration of the phosphorylated form of the substrate at the center, $c_A(0)$, as shown in Figure 1. While the length of the gradient is determined by the phosphatase reaction rate constant and the diffusion coefficient (Equation 1), the actual molar concentration of the phosphorylated form of the substrate at the plasma membrane is determined largely by the kinase reaction rate constant [9, 11]. In the limit of a very high kinase reaction rate constant, the fraction of substrate that is phosphorylated in the immediate vicinity of the plasma membrane approaches unity [9, 11].

In addition to these local effects, there will be a global effect on the phosphorylation state. Integrating the concentration of the phosphorylated form of the substrate, $c_A(r)$, over the entire cell, we obtained an expression for the average concentration of the phosphorylated form, $<c_A>$, given by Equation 9. As shown in Figure 1, the average concentration of the phosphorylated form decreases with increasing cell size, manifested qualitatively as a shift from a cell that is largely phosphorylated when it is small (i.e., orange/red in Figure 1A) to being largely dephosphorylated when it is large (i.e., blue in Figure 1C). Note that this shift requires that the molar concentration of the phosphatase be held constant and not simply be diluted by the increasing volume. Such constant concentration, albeit with some degree of stochastic fluctuation, is presumably maintained in many situations, and naturally arises when there is zeroth-order synthesis and first-order degradation [17].

The reason for this shift is that it is very difficult for the phosphorylated form of the substrate to diffuse to the

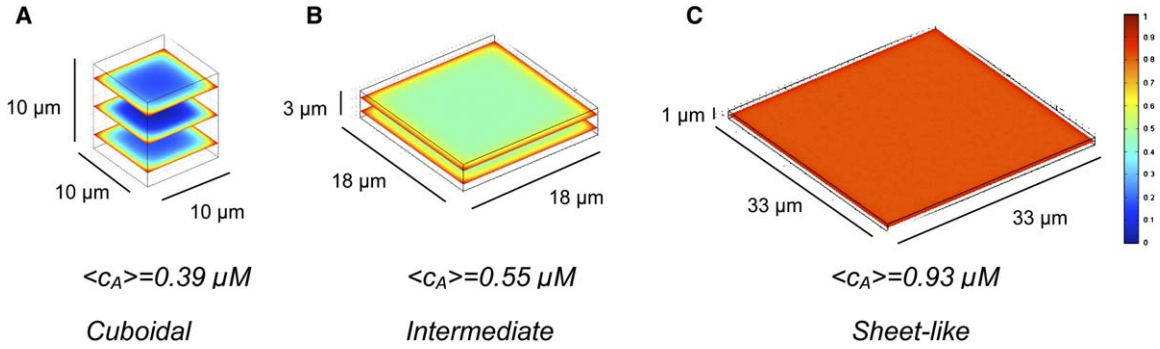

Figure 2. Cell Flattening at Constant Volume Increases Global Phosphorylation Levels

The concentration profile of the phosphorylated form of the substrate is shown for planar slices through rectangular boxes of various thickness, but constant volume. Parameters are the same as in Figure 1.

(A) A cuboidal cell (10 μm × 10 μm × 10 μm = 1000 μm^3) is largely dephosphorylated ($<c_A>$ = 0.39 μM) because the majority of its cytoplasm is more than the gradient decay length away from the plasma membrane. Three planar slices through the 3D finite element solution are shown.

(B) As the cell flattens at roughly constant volume (3 μm × 18 μm × 18 μm = 970 μm^3), a greater fraction of the cytoplasm lies within the gradient decay length of the plasma membrane and so becomes generally more phosphorylated ($<c_A>$ = 0.55 μM). Two planar slices through the 3D solution are shown for this intermediate case.

(C) Further cell flattening (1 μm × 33 μm × 33 μm = 1000 μm^3) results in a sheet-like cell shape where the cytoplasm is nearly all phosphorylated ($<c_A>$ = 0.93 μM). One planar slice through the 3D solution is shown. Thus, as a cell flattens, it switches from being largely dephosphorylated to being largely phosphorylated, even as all other parameters remain constant, including cell volume, kinase rate constant, and phosphatase rate constant.

center of the large cell without first being dephosphorylated. The difficulty is quantified by $L_{gradient}$, which is approximately the average distance that the phosphorylated form of the substrate diffuses before the phosphatase reaction occurs. If the cell is much larger than this distance, then it is very unlikely that the phosphorylated form will make it to the central regions of the cell, and instead it will be confined to a thin region just beneath the plasma membrane, a "shell" of thickness $L_{gradient}$. In chemical reactor analysis and design [18], the characteristic system dimension scaled by the gradient length defines a dimensionless quantity known as the Thiele modulus (see Equation 2). When $\Phi \approx 1$, then the cell is similar in scale to the gradient length, and the cell will be largely phosphorylated. Alternatively, when $\Phi > 1$, then the cell is relatively large and will be largely dephosphorylated. Therefore, a change in the cell size alone will cause a global shift in the phosphostate of the cell, and the Thiele modulus provides a convenient dimensionless quantity with which to characterize the phosphostate regime.

We next considered the consequences of a cell changing its shape while maintaining constant volume. Such changes are common during cell adhesion and migration, both in vivo and in vitro, as mediated by assembly and rearrangement of the cytoskeleton in concert with extracellular adhesion molecules [19]. For simplicity, we treated the cell as a cube, and then calculated its phosphostate as it flattened in one dimension and spread equally in the other two dimensions, all while maintaining constant volume. Again, we assumed that the kinase is associated with the plasma membrane and that the phosphatase is distributed uniformly throughout the cytoplasm. For example, as an epithelial cell spreads, it shifts from cuboidal to sheet-like (i.e., squamous). As shown in Figure 2, such a model cell becomes progressively more phosphorylated as it flattens. The reason for this is that in a very flat cell, the entire cytoplasm is within a distance $L_{gradient}$ of the plasma membrane. Thus, a cell would change its phosphostate simply by changing its shape. The dependence of phosphorylation on shape could play a role in mediating the phosphorylation changes that occur during the cell cycle, since it is often observed that flat cells round up as they enter mitosis. Note that the membrane curvature per se is not important; the sharp corners of the cube in Figure 2A (which have very high curvature) are only slightly more activated than the adjacent faces of the cube (which are flat). Rather, curvature allows the plasma membrane to fold back onto itself so that two regions of the cytoplasm can face each other and activate the intervening cytoplasm (provided the gap between the two regions is smaller than $L_{gradient}$). A common principle in these first two examples is that for a particular shape (e.g., a sphere or rectangular box), the larger the surface-to-volume ratio, the greater the fraction phosphorylated.

Cells frequently exhibit asymmetry in their shape so that there is a defined axis of polarity with a leading edge and a trailing edge [19]. Cell polarity is established and maintained by the cytoskeleton in response to the local chemical and mechanical environment. We therefore considered the consequences of cell polarity for the phosphostate of the cell. For simplicity, we treated the cell as a three-dimensional triangle (i.e., a wedge) and then calculated the phosphostate as a function of the asymmetry in the position of the peak of the triangle. As shown in Figure 3, as a cell changes its shape from symmetric to asymmetric, it induces a high degree of phosphorylation in the thin, leading edge of the cell relative to the thicker trailing edge. Note also that in the symmetric case, the edge of the cell is more highly phosphorylated than the center of the cell. The same principles identified in the cell flattening example apply here as well: in the thin leading edge, the dorsal and ventral membrane surfaces are closely apposed to one another, whereas in the thick trailing edge they are relatively distant from one another.

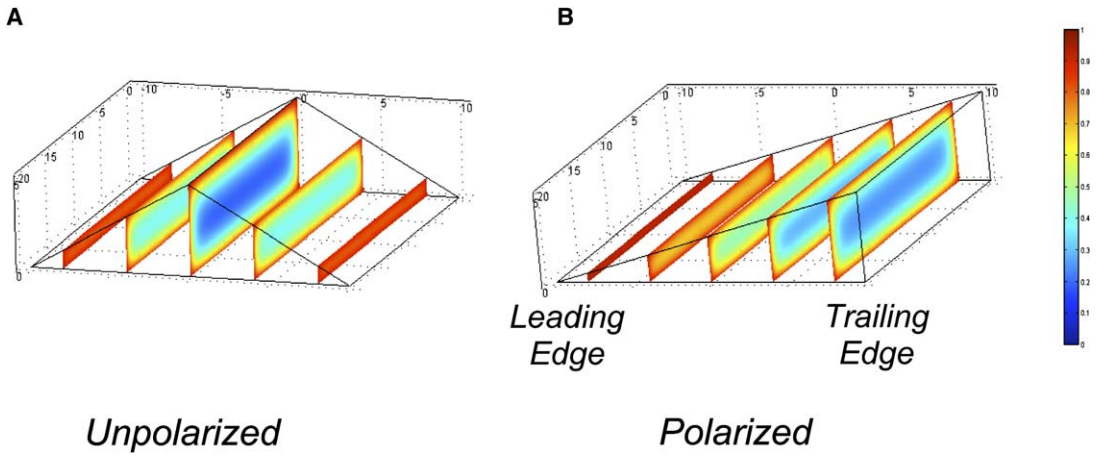

Figure 3. Cell Polarization Results in Phosphorylation at the Leading Edge and Dephosphorylation at the Trailing Edge

With the parameters from Figure 1, the concentration of the phosphorylated form of the substrate was calculated for both unpolarized and polarized cells. Cell width = 20 μm, length = 20 μm, height = 5 μm.

(A) An unpolarized cell is largely phosphorylated at its edges, especially where the angles are acute. However, there is no asymmetry in phosphorylation with respect to the polarity axis in the asymmetric cell. Five planar slices through the 3D solution are shown.

(B) As a cell becomes polarized, the leading edge becomes relatively thin compared to the trailing edge and so the leading edge becomes highly phosphorylated, while the trailing edge becomes largely dephosporylated. The leading edge is highly phosphorylated because the cytoplasm it contains is all within the gradient decay length of the plasma membrane, whereas at the trailing edge the cytoplasm is generally more distant from the plasma membrane. Five planar slices through the 3D solution are shown. Thus, cell polarization, characterized by a thin leading edge and a thick trailing edge, will naturally result in a relatively phosphorylated leading edge and dephosphorylated trailing edge.

From the analysis of spread and polarized cells, it is apparent that the cytoplasm within any thin protrusion, such as a filopodium that has a relatively small diameter of ~1 μm, will be highly phosphorylated. Computer simulations confirm this expectation and show that the cytoplasm contained within the filopodium is highly phosphorylated even as the adjacent cytoplasm remains highly dephosphorylated, as shown in Figure 4. Thus, the cell can differentiate its cytoplasm into two biochemically distinct regions simply by extending a narrow cytoplasmic protrusion. These results suggest that it would actually be the norm that the biochemistry of these cytoplasmic extensions be dissimilar from the bulk of the cytoplasm. Furthermore, these results are general in that the same principles should apply to other cytoplasmic extensions, such as axons, flagella, cilia, and stereocilia. Again, these compartments would be expected to be intrinsically distinct, in terms of their cytoplasmic biochemistry, from the bulk cytoplasm from which they extend.

Finally, we wished to compare the model to experimental data. It is currently of interest to develop probes that report not only the localization of G proteins and phosphoproteins, but also their activation as a function of time and space in living cells [3, 20, 21]. There is presently only limited data on the activation dynamics, but a common observation is the existence of activation gradients in the cell. As a specific example, we considered the activation of Cdc42, a member of the Rho family of small GTPases. Recently, Nalbant et al. [12] experimentally measured the activation of Cdc42 in cultured fibroblasts by using a fluorescent probe they developed, called MeroCBD, that fluoresces strongly when bound to activated Cdc42 (GTP-Cdc42). With MeroCBD-injected fibroblasts, Nalbant et al. [12] found that Cdc42 activation is greatest at the leading edge in extending protrusions. However, they did not identify a specific mechanism that might give rise to the localization of Cdc42 activity to the cell perimeter. To test whether the principles that we outlined above might play at least some role in achieving the experimentally observed activation of Cdc42, we obtained the original cell thickness (GFP signal) and activation (MeroCBD signal) data, and then we predicted the relative activation of Cdc42 as a function of the pixel position by means of Equation 11.

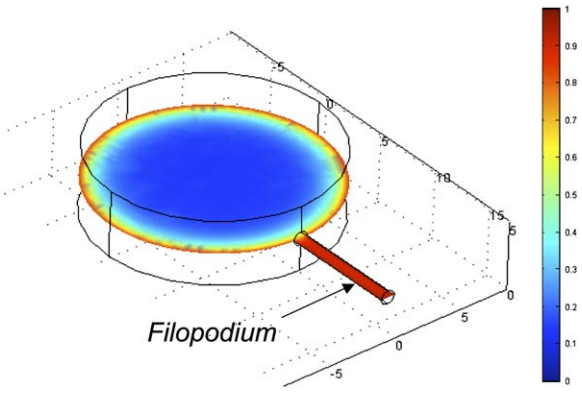

Figure 4. Thin Protrusions Will Be Highly Phosphorylated

With the parameters from Figure 1, the concentration of the phosphorylated form of the substrate was calculated for a cylindrical cell (radius = 8 μm, height = 5 μm) having a single cylindrical filopodium extending from it (radius = 0.5 μm, length 8 μm). A single planar slice is shown through the midpoint of the 3D solution. The filopodium is highly phosphorylated, while the bulk cytoplasm is generally dephosphorylated. Thus, it is expected that a thin process, such as a filopodium, axon, flagellum, or cilium, will have a phosphostate distinct from the rest of the cell. In addition, simply by extending many thin processes, the cell could shift to a state that is globally more phosphorylated.

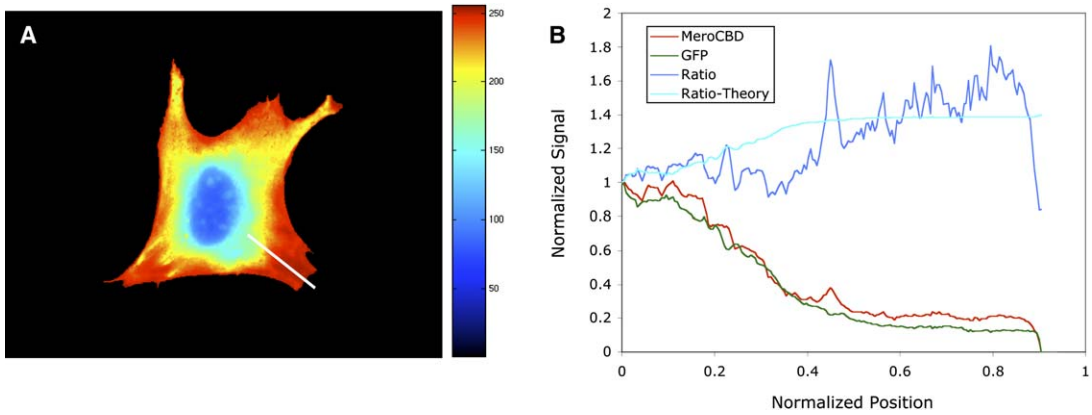

Figure 5. Model Predictions for Cdc42 Activation in Fibroblasts

With the data obtained by Nalbant et al. [12], the activation of Cdc42 was simulated with the experimentally observed cell thickness data as the input to the model.

(A) Simulated activation of Cdc42 with the GFP data of Nalbant et al. (Figure 2C in [12]) as input to the model. The activity of Cdc42 is predicted to be greatest near the edge of the cell (compare to Figure 2A in [12]).

(B) Inverse correlation of Cdc42 with cell thickness. Taking a line scan across the lower right portion of the cell in (A) (i.e., along the white line in [A]) that runs from the perinuclear region to the cell perimeter, the experimental ratio of MeroCBD fluorescence (activated Cdc42 reporter) to GFP fluorescence (cell thickness reporter) was measured in arbitrary fluorescence units. From these data, a ratio was calculated and then the model used to approximate the experimental data. As predicted by the model, the Cdc42 activity (measured by the ratio) is greatest where the cell is thinnest (measured by GFP).

Note that we confirmed the validity of the slab geometry solution by Monte Carlo simulation of the three-dimensional reaction-diffusion problem (not shown). With this approach, we were able to predict the extent of Cdc42 activation on a pixel-by-pixel basis to generate a simulated image of the MeroCBD signal, as shown in Figure 5A. We found that the model-predicted simulated image successfully reproduces the general behavior that was observed experimentally by Nalbant et al. [12] (compare our simulated image in Figure 5A to Nalbant et al.'s experimental image in their Figure 2A). Specifically, the model predicts that Cdc42 activation should be greatest where the cell is thinnest, which is generally near the edges of the cell, and lowest where the cell is thickest, generally near the nucleus. There is generally a good, but not perfect, inverse correlation between the extent of activation and the cell thickness as shown by the line scan profile in Figure 5B. The origin of the discrepancies may be (1) noise and nonlinearity in the experimental signal and (2) variability in local microtubule mass or microtubule plus end concentration (found by Nalbant et al. [12] to globally potentiate Cdc42 activation). In addition, Nalbant et al. [12] observed that overall Cdc42 activity increased during cell spreading (Figures 3A and 3B in [12]), as predicted by the model (Figure 2). Overall, the model captures the general features of Cdc42 activation in fibroblast cells as measured by MeroCBD fluorescence.

Discussion

Our analysis shows that cell size and shape are expected to influence phosphorylation level locally and globally. In the results presented above, it was assumed that the kinase was tethered to the plasma membrane, while the phosphatase was homogeneously distributed in the cytoplasm. The conclusions drawn here do not depend on such a specific arrangement, only that the two enzymes be spatially distinct from each other. When spatially segregated, then the intervening space will serve as a battleground upon which the antagonistic phosphorylation and dephosphorylation reactions are carried out, with the kinase winning the battle in its vicinity, and the phosphatase winning in its vicinity. When the cell changes shape, for example through the underlying dynamics of the cytoskeleton, two surfaces can come close to one another, allowing the surface-associated enzyme to prevail locally. If this enzyme is a kinase, then the local state will be phosphorylated. If the enzyme is a phosphatase, then the local state will be dephosphorylated. In either case, the local phosphostate will be different from that of the bulk cytoplasm. So the conclusions drawn do not depend on the kinase being at the plasma membrane, only that its location be distinct from the phosphatase. It is important to note that if the kinase and phosphatase are colocalized, then the gradients disappear altogether. For example, if both the kinase and phosphatase are associated with the plasma membrane, then there will be no gradient of phophostate within the cell. Similarly, if the kinase and phosphatase are both freely diffusing in the cytoplasm, then there will again be no gradient. So, in principle, gradients can be turned on and off simply by redistribution of one of the two enzymes to a specific structure not accessible to the other. In some intermediate cases, the two enzymes might be very close to each other, but not exactly colocalized. In this case, the gradient will exist in the intervening space, but if this distance is much less than $L_{gradient}$, then the gradient will be very small and the phosphostate effectively uniform throughout the cell.

The model developed here is intentionally simplified to illustrate the underlying principles. In any particular signaling pathway, it will be important to consider the myriad complexities that will enter into the analysis. These complexities include nonlinear kinetics of activation and

deactivation (e.g., second-order or higher-order reaction kinetics), spatially varying diffusion coefficients, spatially distributed activators and deactivators, stochastic fluctuations in copy number, and parallel pathways for activation and deactivation, to name a few. In this regard, it will be especially interesting to consider the effects of nonlinear deactivation as a means of achieving gradients that lack a particular length scale at distances far from the activation reaction, as theoretically outlined recently for extracellular morphogen gradients decaying via self-enhanced degradation [22]. Regardless of the details of the kinetic scheme, as long as a particular component of a signaling pathway has spatially segregated activators and deactivators, then there will exist a spatial gradient of activation with a length scale at which the concentration is some fraction of the maximum (e.g., half-maximal). If this length scale is similar to the length scale of the cell or smaller, then the size- and shape-dependent effects described here can be expected to influence the extent to which the signaling pathway is active, both locally and globally.

Perhaps the strongest experimental evidence of G protein state gradients comes from the studies reported by Nalbant et al. [12]. By using a fluorescent probe that they called MeroCBD, they observed the activation of Cdc42, a member of the Rho-family of small GTPases, in living fibroblasts. They observed that the activation of Cdc42 was highest at the cell edge, where the cell is thinnest. The authors did not offer a mechanistic explanation for the observation, because it is not clear in general how the cell identifies its leading edge. Their observation of high activation at the leading edge is consistent with the general prediction of our modeling (Figure 3) and was confirmed to be consistent with the cell thickness data obtained by Nalbant et al. (Figure 2 in [12]) as a direct input into our model. Comparison of our model output (Figure 5) to the actual experimental output (Figure 2 in [12]) confirms that the basic assertion of the model is consistent with the experimental observations. In addition, the model predicts (Figure 2) the observed global increase in Cdc42 activation upon cell spreading (Figure 3 in [12]). So the model successfully predicts the basic features of Cdc42 activation in fibroblasts.

We do not claim that the model outlined here explains all features of Cdc42 activation. For example, Nalbant et al. [12] observed that the activation in filopodia was lower than the adjacent lamellipodial regions (see Figure 3C in [12]), which is inconsistent with the present model (Figure 4). This inconsistency suggests that a component that is required for Cdc42 activation is present in lamellipodia but is absent from filopodia. The analysis of Nalbant et al. [12] suggests that a key regulator of Cdc42 activation may be the microtubule cytoskeleton, since nocodazole (which depolymerizes microtubules) diminishes the overall activation of Cdc42, whereas cytochalasin D (which depolymerizes actin filaments) has little effect on Cdc42 activation. Since microtubules invade filopodia less frequently than lamellipodia, it may be that microtubule plus ends provide a factor that is necessary for efficient Cdc42 activation. Thus, the recruitment of microtubules, which is necessary to establish cell polarity, may deliver a stimulus that triggers actin protrusion via localized Cdc42 activation. This new protrusion then provides microtubules with new intracellular space to explore, and a feedback loop is created. This feedback loop would be broken if the protrusion failed to provide adequate signals to promote the net assembly of microtubules, which is necessary in order for the protrusion to retain invading microtubules. Such a feedback mechanism may explain why some regions of the cell edge were more activated than others (see Figures 3 and S5 in [12]). Clearly, the present model is not the only model that could explain the experimentally observed Cdc42 activation. Rather, it is more appropriate to merely conclude that the model successfully predicts the general behavior of spatial gradients of Cdc42 activation, the basis of which is unclear at the moment, with fairly simple arguments.

The strongest evidence documenting the existence of phosphostate gradients comes from an analysis of the spatial distribution of the phosphostate of Op18/stathmin [3], a regulator of microtubule dynamics that is overexpressed in a number of cancers and that mediates neuron growth [23]. By using fluorescence resonance energy transfer-based probes that were specific to either the phosphorylated or dephosphorylated forms of Op18/stathmin, Niethammer et al. were able to visualize gradients in the phosphostate of Op18/stathmin in mitotic and interphase *Xenopus* cell lines [3]. In interphase cells, Op18/stathmin is relatively phosphorylated in the leading edge of the migrating cells. To explain this asymmetry, Niethammer et al. [3] postulated that upstream regulators of Op18/stathmin, such as Rac1/Pak, are localized to the leading edge. This explanation is supported by the observation that microtubule assembly, which is promoted when Op18/stathmin is phosphorylated [23], is favored near the leading edge of migrating cells and that suppressing the Rac1/Pak pathway suppressed the assembly of microtubules near the leading edge [24]. Our results here demonstrate that it is not necessary to invoke such localization. Rather, simply by extending a thin lamellipodium from the edge of the cell, the Rac1/Pak pathway (or other unknown Op18/stathmin regulatory pathways) may be locally activated, as illustrated in Figure 3, without any requirement for redistribution of upstream regulators to the leading edge. As argued above in the case of Cdc42 activation, microtubules may play an important role in establishing a feedback mechanism between actin-based protrusion and microtubule invasion/retention at the leading edge.

The present results provide an explanation for how cells can regulate and control their activities as a function of their size and shape. Previous experimental work by Ingber, Chen, and coworkers demonstrated that cell fate can be determined by cell shape [15, 16, 25]. For example, bovine aortic endothelial cells cultured on micropatterned islands switch from growth to apoptosis as they change from well-spread to rounded, even when the total surface area available for interaction with the adhesive surface is held constant. How a cell could sense its own shape has remained enigmatic, but one possibility is that cells that are well-spread have a greater internal mechanical tension within their cytoskeleton, perhaps via RhoA-mediated contractility, as compared to rounded cells [16]. Even so, this is not likely to be the entire explanation, since RhoA activity

by itself is not able to control human mesenchymal stem cell differentiation, indicating that shape itself is still important [16]. Our results suggest that cell shape could be sensed by the close apposition of membranes that occurs in flat cells to turn on the global phosphorylation of substrates whose activators are plasma membrane associated and whose deactivators reside in the bulk cytoplasm, as shown in Figure 2.

In a similar vein, the shape dependence of phosphostate could be used to mediate mechanosensing. For example, as a cell is subjected to a mechanical stress, such as fluid shear stress on endothelial cells [26] or tensional stress on neurons [27–29], it deforms. These deformations could then be used to locally or globally activate or inactivate signaling pathways, as shown in Figures 2–4. That mechanosensing could occur simply through changes in the size of an extracellular compartment has recently been established in the case of normal human bronchial epithelial cells subjected to compressive stress in vitro [30]. Tschumperlin et al. demonstrated that changes in the volume of the intercellular space create changes in the concentration of an extracellular autocrine ligand, which in turn controls downstream signaling pathways [30]. Subsequent analysis by Maly et al. showed that similar extracellular mechanisms could play a role in EGFR autocrine signaling in cardiac tissue [31]. A separate study by Maly et al. established also that spatial asymmetry in the presentation of an extracellular ligand would be predicted to result in intracellular gradients of the second messengers [32]. However, these studies did not consider the theoretical consequences of changes in the size or shape of the cell itself in the signaling process. The present results demonstrate that cell size and shape by themselves are expected to influence the signaling process both locally and globally, as long as the antagonistic enzymes are spatially segregated from each other.

In this light, the analysis of signaling pathways requires consideration of the physical size and shape of the environment within which they occur. For example, in the bacterial chemotaxis pathway, the activation of flagellar motors, which are distributed approximately at random over the plasma membrane, depends on the binding of phosphorylated CheY, which is generated by the signaling complex located at the anterior end of the cell and consumed there as well [33]. It is worth noting that the ATP consumption rate of CheY is expected to be appreciable, since there are $\sim$8000 molecules of CheY in the bacterium (volume $\sim 2\ \mu m^3$) and the average cycle time of CheY phosphorylation-dephosphorylation is $\sim$2 s [33]. This results in a potential consumption rate of ATP of $\sim$2000 ATP/μm^3 s via this signaling pathway. Such high consumption rates are needed if the cell is to maintain gradients on the micrometer scale and if the signaling system is to respond rapidly (seconds). Apparently such an energy demand is worthwhile from the point of view of the bacterium because it enables the bacterium to avoid toxins and locate food sources.

Were the activator and deactivator not colocalized, then a spatial gradient in phosphorylated CheY is expected to develop such that motors close to the signaling complex are more likely to be activated than those that are farther away [33]. As the cell grows, the motors would be expected to be, on average, progressively farther from the signaling complex. This will have the effect of making the cell progressively less motile, especially if the effector of the signaling pathway has a highly allosteric response to the signal, as is the case for the bacterial flagellar motor [34]. If larger cells were to evolve from smaller cells, then they would need to also evolve their signaling systems to avoid being placed at a competitive disadvantage relative to their ancestral cells in terms of food accumulation and avoidance of toxins. So it may be that the colocalization of activators and deactivators is important for suppressing gradients in some contexts [33]. The high consumption rate of ATP in either case can be used to support rapid response, with or without a spatial gradient.

In summary, it is expected that models that treat cell signaling as simply a network of spatially homogeneous reactions will not be able to accurately predict the extent to which a given signaling pathway will be active. Therefore, to fully understand signaling pathways, and their evolution, it seems that it will be necessary to incorporate cell size and shape into the analysis.

Experimental Procedures

Governing Equations and Boundary Conditions

The governing equation for all the geometries considered was that of three-dimensional diffusion and first-order phosphatase reaction at steady-state, which is

$$0 = D\nabla^2 c_A - k_p c_A, \tag{3}$$

where D is the diffusion coefficient, k_p is the first-order phosphatase reaction rate constant, and c_A is the molar concentration of the phosphorylated form of the substrate. Note that the phosphatase reaction kinetics are more generally considered to obey Michaelis-Menten kinetics, which is of the form

$$r_A = -\frac{V_{max} c_A}{K_M + c_A}, \tag{4}$$

where r_A is the rate of disappearance of the phosphorylated form, V_{max} is the maximum rate of the reaction (proportional to the enzyme concentration), and K_m is the Michaelis-Menten constant. When $c_A << K_m$, then the kinetics become first-order

$$r_A = -\frac{V_{max}}{K_m} c_A = -k_p c_A, \tag{5}$$

where the ratio of V_{max} to K_m defines k_p. In the opposite limit when $c_A \gg K_m$, then the kinetics become zeroth-order

$$r_A = -V_{max}. \tag{6}$$

In between these regimes, the kinetics are of a fractional order (between 0 and 1). Since the zeroth-order solutions behave similarly to the first-order solutions (not shown), and the transition between them is gradual, we used first-order kinetics for simplicity. Under some circumstances, the kinetics may be higher than first-order, such as the second-order kinetics associated with dimerization. In this case, the solution will still decay in a manner qualitatively similar to zeroth- and first-order kinetics, but it will decay more rapidly. Such kinetic schemes require numerical solutions, but will still have a characteristic length scale for the decay. Provided the length scale is comparable to that of the cell, or smaller, then the principles described here apply. We focused on Michaelis-Menten kinetics in this initial report because they describe the kinetics of enzymes, which are believed to mediate the deactivation reactions. Typical values of K_m for phosphatases range from 0.1 to 20 μM [11].

The boundary condition is at the plasma membrane, which is the physical boundary to the reaction-diffusion system, where there is a balance between the kinase reaction rate that is localized to the

plasma membrane and the diffusive flux of the phosphorylated form of the substrate. Specifically, this can be written as

$$0 = -D(\bar{n} \bullet \nabla c_A)|_{boundary} + k_{kin} c_B|_{boundary}, \quad (7)$$

where $\bar{n}$ is the vector normal to the plasma membrane surface, k_{kin} is the first-order kinase reaction rate constant, and c_B is the molar concentration of the dephosphorylated form of the substrate. Note that the kinase reaction is treated as first-order for the same reasons described above for the phosphatase reaction. Conservation of the substrate requires in this model that

$$c_T = c_A + c_B, \quad (8)$$

where c_T is the total molar concentration of the substrate, which is everywhere a constant.

Analytical Solution to the Average Concentration within a Sphere

The concentration profile of the phosphorylated form of the substrate has been solved analytically for a sphere [11] and for rectangular coordinates in one dimension [9]. These relations allow one to calculate the local concentration of the phosphorylated form of the substrate. In addition to these local effects, there will be a global effect on the phosphorylation state. Integrating the concentration of the phosphorylated form of the substrate, $c_A(r)$, over the entire spherical cell, we obtained an expression for the average concentration of the phosphorylated form, $\langle c_A \rangle$ in a sphere, which is given by

$$\langle c_A \rangle = \frac{6C_1}{R}\left[\frac{\cosh\Phi}{\Phi} - \frac{\sinh\Phi}{\Phi^2}\right], \quad (9)$$

where C_1 is an integration constant defined by

$$C_1 = \frac{k_{kin} c_T R^2}{\left[3D\left(1/L_{gradient} - 1/R\right) + k_{kin}R\right]e^{\Phi} + \left[3D\left(1/L_{gradient} + 1/R\right) - k_{kin}R\right]e^{-\Phi}} \quad (10)$$

and Φ is the Thiele modulus (used in chemical reactor analysis [18]), here defined as in Equation 2. Equation 9 was used to generate Figure 1.

Analytical Solution to the Average Concentration within a Slab

By using the same approach of integration as described above for a sphere, we obtained an expression for the average concentration in a slab, which is given by

$$\langle c_A \rangle = \frac{c_T}{\Phi}\left[A\left(1 - e^{-\Phi}\right) + B\left(e^{\Phi} - 1\right)\right], \quad (11)$$

where

$$A = \Phi^* e^{2\Phi} / \left[\Phi\left(e^{2\Phi} - 1\right) + \Phi^*\left(e^{2\Phi} + 1\right)\right]$$
$$B = \Phi^* / \left[\Phi\left(e^{2\Phi} - 1\right) + \Phi^*\left(e^{2\Phi} + 1\right)\right], \quad (12)$$

$$\Phi = \sqrt{\frac{k_p L^2}{D}}$$
$$\Phi^* = \frac{k_{kin} L}{D}, \quad (13)$$

and L is half the thickness of the slab. These relations were used to calculate the relative activation of Cdc42 in fibroblast cells, which are very thin relative to their width.

Finite Element Solutions

For nonspherical objects, the solution to the reaction-diffusion problem was obtained by numerical integration with a commercially available solver (FEMLab 3.1i, Comsol, Inc., Burlington, MA) running on a dedicated workstation (Sun Blade 2000, Sun Microsystems, Inc., Santa Clara, CA). Typically, 15,000–25,000 elements were used and a single solution required 30–60 s. The finite element solution was used to generate the full three-dimensional solution, and then a limited number of planar slices through the solution was obtained to generate Figures 2–4.

Acknowledgments

The authors thank L. Hodgson and K. Hahn for providing their original MeroCBD fibroblast data, B. Earnshaw and J. Howard for helpful comments, V. Barocas for technical assistance with the finite element modeling and helpful discussions, and the Minnesota Supercomputing Institute for providing computing resources. This article is dedicated to the memory of Raymond A. Odde, P.E. The work was supported partially by a grant from the National Science Foundation (BES-0119481) and from the National Institutes of Health (GM-71522).

Received: June 7, 2006
Revised: July 14, 2006
Accepted: July 21, 2006
Published: September 5, 2006

References

1. Turing, A.M. (1952). The chemical basis of morphogenesis. Philos. Trans. R. Soc. Lond. B Biol. Sci. *237*, 37–72.
2. Alberts, B., Johnston, A., Lewis, J., Raff, M., Roberts, K., and Walter, P. (2002). Molecular Biology of the Cell, fourth edition (New York: Garland Publishing).
3. Niethammer, P., Bastiaens, P., and Karsenti, E. (2004). Stathmin-tubulin interaction gradients in motile and mitotic cells. Science *303*, 1862–1866.
4. Carazo-Salas, R.E., and Karsenti, E. (2003). Long-range communication between chromatin and microtubules in *Xenopus* egg extracts. Curr. Biol. *13*, 1728–1733.
5. Gruss, O.J., Wittmann, M., Yokoyama, H., Pepperkok, R., Kufer, T., Sillje, H., Karsenti, E., Mattaj, I.W., and Vernos, I. (2002). Chromosome-induced microtubule assembly mediated by TPX2 is required for spindle formation in HeLa cells. Nat. Cell Biol. *4*, 871–879.
6. Gruss, O.J., Carazo-Salas, R.E., Schatz, C.A., Guarguaglini, G., Kast, J., Wilm, M., Le Bot, N., Vernos, I., Karsenti, E., and Mattaj, I.W. (2001). Ran induces spindle assembly by reversing the inhibitory effect of importin alpha on TPX2 activity. Cell *104*, 83–93.
7. Kalab, P., Weis, K., and Heald, R. (2002). Visualization of a Ran-GTP gradient in interphase and mitotic *Xenopus* egg extracts. Science *295*, 2452–2456.
8. Gardner, M., Pearson, C., Sprague, B., Zarzar, T., Bloom, K., Salmon, E.D., and Odde, D.J. (2005). Tension-dependent regulation of microtubule dynamics at kinetochores can explain metaphase congression in yeast. Mol. Biol. Cell *16*, 3764–3775.
9. Sprague, B.L., Pearson, C.G., Maddox, P.S., Bloom, K.S., Salmon, E.D., and Odde, D.J. (2003). Mechanisms of microtubule-based kinetochore positioning in the yeast metaphase spindle. Biophys. J. *84*, 3529–3546.
10. Wollman, R., Cytrynbaum, E.N., Jones, J.T., Meyer, T., Scholey, J.M., and Mogilner, A. (2005). Efficient chromosome capture requires a bias in the "Search-and-Capture" process during mitotic spindle assembly. Curr. Biol. *15*, 828–832.
11. Brown, G.C., and Kholodenko, B.N. (1999). Spatial gradients of cellular phospho-proteins. FEBS Lett. *457*, 452–454.
12. Nalbant, P., Hodgson, L., Kraynov, V., Toutchkine, A., and Hahn, K.M. (2004). Activation of endogenous Cdc42 visualized in living cells. Science *305*, 1615–1619.
13. Salmon, E.D., Saxton, W.M., Leslie, R.J., Karow, M.L., and McIntosh, J.R. (1984). Diffusion coefficient of fluorescein-labeled tubulin in the cytoplasm of embryonic cells of a sea urchin: video image analysis of fluorescence redistribution after photobleaching. J. Cell Biol. *99*, 2157–2164.
14. Jacobson, K., and Wojcieszyn, J. (1984). The translational mobility of substances within the cytoplasmic matrix. Proc. Natl. Acad. Sci. USA *81*, 6747–6751.
15. Chen, C.S., Mrksich, M., Huang, S., Whitesides, G.M., and Ingber, D.E. (1997). Geometric control of cell life and death. Science *276*, 1425–1428.
16. McBeath, R., Pirone, D.M., Nelson, C.M., Bhadriraju, K., and Chen, C.S. (2004). Cell shape, cytoskeletal tension, and RhoA regulate stem cell lineage commitment. Dev. Cell *6*, 483–495.

17. Paulsson, J. (2004). Summing up the noise in gene networks. Nature *427*, 415–418.
18. Froment, G.F., and Bischoff, K.B. (1990). Chemical Reactor Analysis and Design, second edition (New York: John Wiley & Sons, Inc.).
19. Ridley, A.J., Schwartz, M.A., Burridge, K., Firtel, R.A., Ginsberg, M.H., Borisy, G., Parsons, J.T., and Horwitz, A.R. (2003). Cell migration: integrating signals from front to back. Science *302*, 1704–1709.
20. Pertz, O., and Hahn, K.M. (2004). Designing biosensors for Rho family proteins—deciphering the dynamics of Rho family GTPase activation in living cells. J. Cell Sci. *117*, 1313–1318.
21. Fujioka, A., Terai, K., Itoh, R.E., Aoki, K., Nakamura, T., Kuroda, S., Nishida, E., and Matsuda, M. (2006). Dynamics of the RAS/ERK MAPK cascade as monitored by fluorescence probes. J. Biol. Chem. *281*, 8917–8926.
22. Eldar, A., Rosin, D., Shilo, B.Z., and Barkai, N. (2003). Self-enhanced ligand degradation underlies robustness of morphogen gradients. Dev. Cell *5*, 635–646.
23. Cassimeris, L. (2002). The oncoprotein 18/stathmin family of microtubule destabilizers. Curr. Opin. Cell Biol. *14*, 18–24.
24. Wittmann, T., Bokoch, G.M., and Waterman-Storer, C.M. (2003). Regulation of leading edge microtubule and actin dynamics downstream of Rac1. J. Cell Biol. *161*, 845–851.
25. Singhvi, R., Kumar, A., Lopez, G.P., Stephanopoulos, G.N., Wang, D.I.C., Whitesides, G.M., and Ingber, D.E. (1994). Engineering cell shape and function. Science *264*, 696–698.
26. Davies, P.F., Zilberberg, J., and Helmke, B.P. (2003). Spatial microstimuli in endothelial mechanosignaling. Circ. Res. *92*, 359–370.
27. Bray, D. (1984). Axonal growth in response to experimentally applied mechanical tension. Dev. Biol. *102*, 379–389.
28. Zheng, J., Lamoureux, P., Santiago, V., Dennerll, T., Buxbaum, R.E., and Heidemann, S.R. (1991). Tensile regulation of axonal elongation and initiation. J. Neurosci. *11*, 1117–1125.
29. Fass, J.N., and Odde, D.J. (2003). Tensile force-dependent neurite elicitation via anti-β1 integrin antibody-coated magnetic beads. Biophys. J. *85*, 623–636.
30. Tschumperlin, D.J., Dai, G., Maly, I.V., Kikuchi, T., Laiho, L.H., McVittie, A.K., Haley, K.J., Lilly, C.M., So, P.T., Lauffenburger, D.A., et al. (2004). Mechanotransduction through growth-factor shedding into the extracellular space. Nature *429*, 83–86.
31. Maly, I.V., Lee, R.T., and Lauffenburger, D.A. (2004). A model for mechanotransduction in cardiac muscle: effects of extracellular matrix deformation on autocrine signaling. Ann. Biomed. Eng. *32*, 1319–1335.
32. Maly, I.V., Wiley, H.S., and Lauffenburger, D.A. (2004). Self-organization of polarized cell signaling via autocrine circuits: computational model analysis. Biophys. J. *86*, 10–22.
33. Lipkow, K., Andrews, S.S., and Bray, D. (2005). Simulated diffusion of phosphorylated CheY through the cytoplasm of *Escherichia coli*. J. Bacteriol. *187*, 45–53.
34. Bray, D., and Duke, T. (2004). Conformational spread: the propagation of allosteric states in large multiprotein complexes. Annu. Rev. Biophys. Biomol. Struct. *33*, 53–73.